PAPER

Check for updates

Site occupancy preference, electrical transport property and thermoelectric performance of Ba$_8$Cu$_{6-x}$Ge$_{40+x}$ single crystals grown by using different metal fluxes†

Jiazhen Wu,[*a] Jingtao Xu ⓘ [*b] and Katsumi Tanigaki[*ac]

Different fluxes, Ga, Bi, In, Sb, and Sn, have been used to grow clathrate Ba$_8$Cu$_{5.3}$Ge$_{40.7}$ (BCG) single crystals using a flux method, and BCG single crystals have been successfully synthesized by Bi-, In- and Sn-flux. The grown crystals were characterized by single crystal and power X-ray diffraction as well as energy dispersive X-ray spectroscopy measurements. The solubility of flux inside the crystals was determined and the actual chemical composition was decided to be: Ba$_8$Cu$_{5.1}$Ge$_{40.5}$ (BCG-Bi), Ba$_8$Cu$_{4.6}$In$_{1.4}$Ge$_{40.0}$ (BCG-In) and Ba$_8$Cu$_{5.1}$Ge$_{40.2}$Sn$_{0.7}$ (BCG-Sn) for the compounds grown from Bi-, In- and Sn-flux, respectively. A high electron mobility (μ), 44.8 cm^2 V^{-1} s^{-1} at 300 K, is observed for BCG-In, which is almost 5 times higher than the reported data at a similar carrier concentration. Therefore, enhanced thermoelectric power factors and *ZT* values are obtained. The relationship between the structure and electrical/thermoelectric properties is discussed. The high μ is most probably due to the relatively ordered cage framework structure in BCG-In, because the 6c site is fully occupied by Cu and In, and the other two sites are uniformly occupied by Ge.

Introduction

Intermetallic clathrates are classified as a type of the conceptual "phonon-glass electron-crystal" (PGEC) materials and have been widely studied for their thermoelectric applications.[1] Among the clathrate family, type-I clathrates (as shown in Fig. 1) are the most extensively considered due to their stable structures and variety of species. From the viewpoint of thermoelectric performance, which can be quantitatively expressed by the dimensionless figure of merit, $ZT = (S^2\sigma/\kappa)T$, the most advantageous point of type-I clathrates is the guest atom vibration modes (rattling), because they can suppress heat conduction efficiently while exert little influence on electrical conduction. Here S, σ, and κ stand for the Seebeck coefficient, electrical conductivity, and thermal conductivity, respectively.

Under the guideline of the PGEC concept, researchers have obtained the highest *ZT* of 1.35 at 900 K for Ba$_8$Ga$_{16}$Ge$_{30}$ (BGG);[2] however, most clathrates still show *ZT* values below 0.5,[1] which is not sufficient for real applications. Therefore,

both optimization of thermoelectric performance and the inspiration from the PGEC character of clathrates are the key issues in the research field. The PGEC concept itself provides two routes for maximizing *ZT*: one is *via* phonon engineering, the other is *via* conduction carrier engineering. On phonon aspect, κ can be further lowered by increasing anharmonicity of the rattling motions, and the typical examples are Ba$_8$Ga$_{16}$Sn$_{30}$ (BGSn), Sr$_8$Ga$_{16}$Ge$_{30}$ (SGG) and p type BGG.[3,4] There are many reported works, in which, rattling phonons and their roles on heat conduction have been described clearly.[5–9] It is noteworthy that the nano-structuring technique, widely applied for other materials systems for suppressing heat conduction,[10,11] do not work well in clathrates and higher *ZT* values were observed in clathrate single crystals,[2,12] indicating that phonon scattering due to rattling phonons is dominant in the scattering process. On the contrary, in order to improve electrical conduction, nano-structuring, which introduces a lot of grain boundaries, should be avoided.

On electron aspect, briefly speaking, the optimization of *ZT* is generally made by modifying three basic physical parameters: the carrier concentration (n), effective mass ($m^\star$) and carrier mobility (μ), because the thermoelectric parameters S, σ and the thermal conductivity contributed from carriers (κ_e) are all strongly associated with these parameters. Among the three parameters, n and $m^\star$ are more closely related to intrinsic materials properties and their detailed information can be deduced

[a] WPI-AIMR, Tohoku University, Sendai, 980-8577, Japan.
   E-mail: wujzphystu@gmail.com, ichi0014@hotmail.com,
   tanigaki@sspns.phys.tohoku.ac.jp
[b] Ningbo Ruiling Advanced Energy Materials Institute Co., Ltd, Ningbo 315500, China
[c] Graduate School of Science, Tohoku University, Sendai 980-8578, Japan
† Electronic supplementary information (ESI) available. See DOI: 10.1039/d0ma00721h
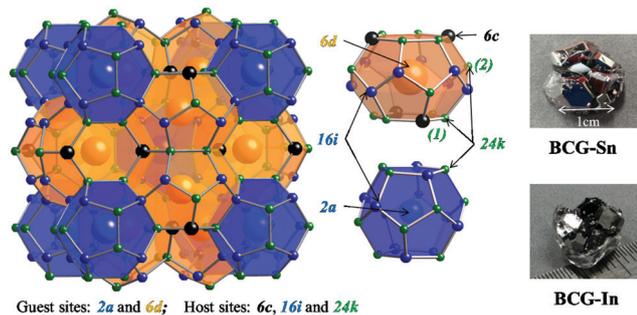
Fig. 1 Crystal structure of type-I clathrate. Atoms in different sites are indicated by different colors. There are two types of cages: dodecahedral cage (blue) and tetrakaidecahedral cage (orange). According to the distance between a guest and a host atom, there are two types of 24k-site atoms: 24k(1) on a six-member ring and 24k(2) which is not on a six-member ring. The grown single crystals of BCG-Sn and BCG-In are shown on the right side.

from electronic band structure; whereas μ is more sensitive to extrinsic factors such as defects and grain boundaries.[10]

The zintl phase concept provides an access to modify n as well as carrier type by deviating the stoichiometric ratio of component elements.[5] For instance, the stoichiometric $Ba_8Ga_{16}Ge_{30}$ is an intrinsic semiconductor, and it can become an n- or p-type conductive compound by increasing the content of Ge or Ga. $m^\star$ can be modified by introducing anharmonic vibrations of the guest atoms[13] or by substituting framework atoms with transition elements.[14] The above modifications on n and $m^\star$ can be summarized as band structure engineering by changing either the Fermi level or the shape of the electronic band. The extrinsic-factor indicator μ can be increased by decreasing the electron scattering rate (τ_e^{-1}), which is closely related to grain boundaries and crystalline defects. In clathrates, μ can actually be enhanced by improving the order of the framework structure as well as the quality of the single crystals as pointed by many researchers.[14–20]

A typical structure of type-I clathrate is shown in Fig. 1. According to the figure, the most ordered framework structure should be made up of one type of element, for example, the frameworks of Ba_8Si_{46} and Ba_8Ge_{46} (actually Ba_8Ge_{43}, with three vacancies on the framework); however these binary compounds are metals and not considered as thermoelectric materials. Relatively ordered framework structures can be created by partial substitution of Si or Ge with group 13 elements (XIII) or transition elements (TM). It has been shown that, in the case of XIII substitution, XIII are randomly distributed in the three framework sites[21] (6c, 16i and 24k as shown in Fig. 1), while in the case of TM substitution, there is a complete ordering of TM on the 6c site.[14,16,17] Among the TM containing clathrates, $Ba_8Cu_{5.3}Ge_{40.7}$ (BCG) was supposed to have the most ordered framework structure, because the stoichiometric amount of Cu is 5.3, which is very close to the number of atoms on the 6c site.[16,17]

Although BCG has been of great scientific interest, reported BCG's are mainly polycrystals, in which grain boundaries as well as framework vacancies greatly limit the electrical transport performance,[16,17] and the advantages of the relatively

ordered structure can not be even evidenced. The difficult point for growing a BCG single crystal is that the useful self-flux method, successfully applied for BGG, SGG, BGSn, *etc.*, can not be used, because none of the component elements could serve as a flux. S. Paschen's group has prepared a single crystal of BCG by using the zone melting method, but they only focused on thermal conductivity.[22] Recently, we have tried tin flux to grow BCG, and obtained beautiful single crystals with good thermoelectric performance (ZT_{max} = 0.6 at 773 K).[23] The flux method provides us a platform to grow high quality single crystals of BCG, so that a comprehensive study using different metal fluxes on crystal quality, site occupancy preference as well as their influences to the electrical and thermal transport properties can be made in details.

In the present study, we report the syntheses, crystal structures and physical properties of $Ba_8Cu_{5.1}Ge_{40.5}$ (BCG-Bi), $Ba_8Cu_{4.6}In_{1.4}Ge_{40.0}$ (BCG-In) and $Ba_8Cu_{5.1}Ge_{40.2}Sn_{0.7}$ (BCG-Sn) single crystals, grown by using Bi-, In-, and Sn-flux, respectively. The influence of different fluxes are carefully analysed by combining the crystal structure and their corresponding physical properties. Comparing to the reported polycrystalline BCG and BGG, our single crystals of BCG show much higher electron mobility and an enhancement of thermoelectric power factor (PF). In particular, the compounds in our study show similar n and $m^\star$, the mere influence of the extrinsic parameter μ can be clearly observed, and this will provide clear and important guidelines for optimizing thermoelectric performance of clathrates.

Experiment section

Materials syntheses

In order to prepare $Ba_8Cu_{5.3}Ge_{40.7}$ single crystals, stoichiometric amounts of Ba pieces (99.9% metal basis), Cu grains (99.99%), and Ge grains (99.999%) with an excess amount of Ba (5% amount) to compensate the reaction loss and a large amount of Bi grains (99.99%) or In grains (99.99%) or Sn grains (99.999%) as the flux, were loaded into a quartz tube in an Ar-filled glovebox [$p(O_2, H_2O) \leq 1$ ppm]. The quartz tube was then sealed under high vacuum and heated in a box furnace up to 1150 °C in 10 h, annealed for 5 h, and slowly cooled down to 650 °C over 100 h and annealed again for 50 h. The liquid flux was then separated from the grown single crystals by centrifugation, and flux impurities can be further removed by using diluted hydrochloric acid or mechanical cutting and polishing. The as grown single crystals of BCG-Sn and BCG-In are shown on the right side of Fig. 1, while BCG-Bi single crystals are very small in size. In the preparation of the materials, different fluxes as well as different amounts of fluxes were tried, the results are summarized in Table 1. BCG polycrystals were prepared by using a radio frequency (RF) induction furnace for comparison.

Microstructure analyses

Selected compounds of BCG-Bi, BCG-In and BCG-Sn single crystals as well as BCG polycrystals were polished and applied

Table 1 The growth result of BCG by using different fluxes. The mole ratio of flux to Ba is x:8

Flux	Amount(x)	Results
Ga	20–40	BGG
Sb	40	Ge pieces
Sn	40	BCG-Sn (<1 mm) and Ge pieces
Sn	20	BCG-Sn (5–11 mm)
In	30–40	BCG-In (5–11 mm)
In	Less than 20	BCG-In (<0.5 mm)
Bi	10–20	BCG-Bi (11 mm) and Ge pieces
Bi	60	Nothing

Table 2 Lattice parameters of BCG single crystals in comparison with the values of polycrystals

Compounds	a/Å	Ref.
BCG-In	10.74576(4)	This work
BCG-Sn	10.71757(3)	This work
BCG-Bi	10.69043(4)	This work
$Ba_8Cu_6Ge_{40}$-poly	10.69154(3)	This work
BCG-Sn	10.71540(3)	23
$Ba_8Cu_{5.3}Ge_{40.7}$	10.69145(5)	17

for field-emission scanning electron microscope (FE-SEM: JEOL, JSM-7800F) measurements and the component elements were analyzed by using energy dispersive X-ray spectrometer (EDS: Oxford Instruments, X-Max SDD Detector) with an accelerating voltage of 20 kV. The following X-ray emission lines were employed for analyses: Ba L, Cu K, Ge K, Sn L, and In L.

Powder X-ray diffraction

The BCG samples were ground into fine powder and loaded in the low background silicon sample holders for powder X-ray diffraction (PXRD) measurement. The data were collected at room temperature (RT) with 2θ ranging from 10° to 90° by using the parallel-beam optics of Rigaku, SmartLab 9MTP. The diffractometer was operated under 40 kV and 50 mA with Cu Kα radiation. Rietveld refinement was performed using GSAS program package.[24,25] Part of the diffraction patterns are shown in Fig. 2 and the calculated lattice constants are summarized in Table 2.

Single crystal X-ray diffraction

The single crystals was checked by a Rigaku R-AXIS single-crystal diffractometer using Mo Kα radiation (λ = 0.71075 Å) at RT. The collected frames were integrated using the Rigaku RAPID AUTO program. Absorption correction was performed by a multi-scan procedure. The crystal structures were solved by direct methods and refined by the full-matrix least-squares method against F_0^2 with WinGX program package.[26] Crystallographic data of BCG single crystals at room temperature can be found in Table 3.

Differential scanning calorimetry

Differential scanning calorimetry (DSC) measurements were made with Netzsch, DSC404F3ST Pegasus. Around 20 mg compounds were sealed in Al_2O_3 ampoules (ϕ 5 mm) and heated up to 1000 °C under an Ar atmosphere with a heating rate of 10 K min^{-1}. BCG-Sn was found to melt congruently at T = 911 °C.[23] The melting points of BCG-In, BCG-Bi, and BCG polycrystals were derived to be T = 918 °C, T = 925 °C, and T = 917 °C, respectively.

Physical properties measurements

Thermoelectric properties of the grown compounds were measured by employing the thermal transport option (TTO) of PPMS (physical properties measurements system, Quantum Design) from 2 K to 300 K. For convenience, the two-probe method was applied. The selected samples were cut into cuboid shapes with dimensions of several millimeters and then attached in copper discs with silver conductive epoxy. The epoxy was dried under vacuum at 150 °C for 2 h to achieve good conductance and high mechanical strength. The resistivity of the compounds was measured with a four-probe method by utilizing the resistivity option of PPMS. Heat capacity measurements were carrier out on BCG-Sn and BCG-In single crystals with mass ranging from 10 mg to 40 mg from 0.36 K to 70 K by using PPMS equipped with a ^{3}He cryostat. Electrical resistivity and Hall resistivity were measured on the same specimen by using the resistivity option of PPMS from 2 K to 300 K. For Hall resistivity measurement, the magnetic field was scanned from ±9 T to 99 T and the sample was polished to be thinner than 0.2 mm. Carrier density and mobility were derived from the electrical transport measurements.

Electronic structure calculations

The electronic band structure calculations were performed using Vienna Ab initio Simulation Package (VASP) program.[27,28] The density functional theory (DFT) in the generalized gradient approximation (GGA) with the Perdew–Burke–Ernzerhof (PBE) functional[29] were used for description of the electronic state. The plane wave basis set with cut-off energy of 500 eV and Γ centered 5 × 5 × 5 Monkhorst–Pack k-point meshes were applied to sample the irreducible Brillouin zone. Structure optimization
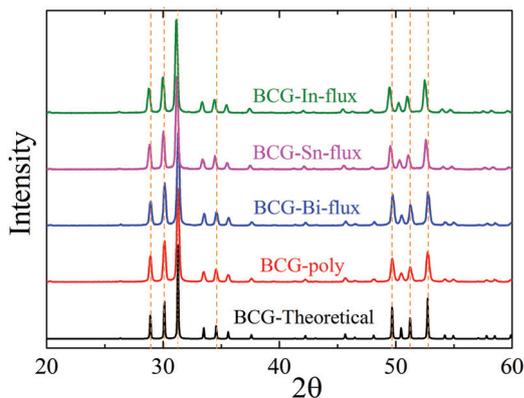

Fig. 2 The X-ray powder diffraction patterns of BCG compounds: BCG-Sn, BCG-In, BCG-Bi, BCG polycrystals, and BCG theoretical calculations. The dashed lines are guides for the eyes to show the shift of the diffraction peaks.

Table 3 Crystallographic data of BCG single crystals at room temperature

Sample	BCG-Sn	BCG-In	BCG-Bi
Space group	$Pm\bar{3}n$ (no. 223)	$Pm\bar{3}n$ (no. 223)	$Pm\bar{3}n$ (no. 223)
a/Å	10.7176(8)	10.7458(5)	10.6904(6)
Molar mass	4424.72	4456.07	4392.45
Z; ρ/g cm^{-3}	1; 5.968	1; 5.963	1; 5.970
Radiation, wavelength λ/Å	0.71075	0.71075	0.71075
Absorption correction	Multi-scan	Multi-scan	Multi-scan
Reflections collected	14 410	4482	3668
Independent reflns	447[$R_{(int)}$ = 0.0601]	279[$R_{(int)}$ = 0.0709]	215[$R_{(int)}$ = 0.0832]
Residuals [$I > 2\sigma(I)$]	R_1 = 0.0268	R_1 = 0.213	R_1 = 0.0304
	wR_2 = 0.0447	wR_2 = 0.0479	wR_2 = 0.0696
Residuals (all data)	R_1 = 0.0285	R_1 = 0.0223	R_1 = 0.0307
	wR_2 = 0.0450	wR_2 = 0.0483	wR_2 = 0.0697
GOF on F^2	1.431	1.178	1.199

was done under BCC symmetry with the electronic energy convergence criterion of $\Delta\varepsilon = 10^{-5}$ eV.

Results and discussion

Phase analyses

The obtained crystals can be recognized through polyhedral surfaces, as shown in Fig. 1. Some Ge pieces were found and separated from clathrate crystals. The composition and crystal structure were then confirmed by EDS and XRD, respectively. The EDS measurements show that a small amount of Sn (In) homogeneously distributes in the BCG-Sn (BCG-In) crystal, while in BCG-Bi, no Bi was detected inside the crystal. Our PXRD results (in Fig. 2) show that the grown compounds are single phases. It means that the small amount of Sn and In are not impurities but the component elements of the compounds. This result can be further confirmed by single crystal X-ray diffraction (SCXRD) and DSC measurements.

Crystal structure and chemical composition

Single crystal X-ray diffraction at RT shows that BCG samples crystallize in cubic space group $Pm\bar{3}n$ (No. 223) with type-I clathrate structure (Fig. 1). The atomic parameters of BCG's are shown in Tables 4–6 for BCG-Sn, BCG-In, and BCG-Bi,

Table 4 Fractional atomic coordinates, site occupancies, and isotropic (U_{eq}) and anisotropic (U_{ij}) atomic displacement parameters at RT for BCG-Sn

Atom	Site	x	y	z	Occupancy	U_{eq}
Ba(1)	2a	0.000	0.000	0.000	1	0.0086(2)
Ba(2)	24k	0.500	0.253	−0.016	0.25	0.023(2)
Cu(1)/Ge(1)	6c	0.250	0.500	0.000	0.849/0.151	0.0098(3)
Ge(2)	16i	0.183(2)	x	x	1	0.0071(7)
Ge(3)/Sn(3)	24k	0.119(9)	0.314(5)	0.000	0.970/0.030	0.0088(1)

Atom	U_{11}	U_{22}	U_{33}	U_{23}	U_{13}	U_{12}
Ba(1)	0.0086(2)	U_{11}	U_{11}	0.000	0.000	0.000
Ba(2)	0.028(4)	0.022(5)	0.021(3)	−0.001(5)	0.000	0.000
Cu(1)/Ge(1)	0.0134(6)	0.0080(4)	0.0080(4)	0.000	0.000	0.000
Ge(2)	0.0071(7)	U_{11}	U_{11}	−0.0010	U_{23}	U_{23}
Ge(3)/Sn(3)	0.0095(2)	0.0086(2)	0.0083(2)	0.000	0.000	0.0013(4)

Table 5 Fractional atomic coordinates, site occupancies, and isotropic (U_{eq}) and anisotropic (U_{ij}) atomic displacement parameters at RT for BCG-In

Atom	Site	x	y	z	Occupancy	U_{eq}
Ba(1)	2a	0.000	0.000	0.000	1	0.0086(3)
Ba(2)	24k	0.500	−0.014	0.252	0.25	0.0285(1)
Cu(1)/In(1)	6c	0.500	0.250	0.000	0.77/0.23	0.0096(5)
Ge(2)	16i	0.183(2)	x	x	1	0.0070(3)
Ge(3)	24k	0.312(5)	0.118(7)	0.000	1	0.0107(3)

Atom	U_{11}	U_{22}	U_{33}	U_{23}	U_{13}	U_{12}
Ba(1)	0.0086(3)	U_{11}	U_{11}	0.000	0.000	0.000
Ba(2)	0.057(1)	0.009(1)	0.020(4)	0.000	0.000	0.000
Cu(1)/In(1)	0.0086(6)	0.0116(8)	0.0086(6)	0.000	0.000	0.000
Ge(2)	0.0070(3)	U_{11}	U_{11}	−0.0009	U_{23}	U_{23}
Ge(3)	0.0107(4)	0.0130(4)	0.0085(4)	0.000	0.000	0.0039(3)

Table 6 Fractional atomic coordinates, site occupancies, and isotropic (U_{eq}) and anisotropic (U_{ij}) atomic displacement parameters at RT for BCG-Bi

Atom	Site	x	y	z	Occupancy	U_{eq}
Ba(1)	2a	0.000	0.000	0.000	1	0.0155(7)
Ba(2)	6d	0.500	0.000	0.250	1	0.0398(7)
Cu(1)/Ge(1)	6c	0.500	0.250	0.000	0.849/0.151	0.0170(8)
Ge(2)	16i	0.183(2)	x	x	0.974(7)	0.0129(6)
Ge(3)	24k	0.314(5)	0.119(8)	0.000	0.998(8)	0.0151(6)

Atom	U_{11}	U_{22}	U_{33}	U_{23}	U_{13}	U_{12}
Ba(1)	0.0155(7)	U_{11}	U_{11}	0.000	0.000	0.000
Ba(2)	0.0457(8)	U_{11}	0.0278(1)	0.000	0.000	0.000
Cu(1)/Ge(1)	0.0156(1)	0.0198(1)	0.0156(1)	0.000	0.000	0.000
Ge(2)	0.0129(6)	U_{11}	U_{11}	−0.0006	U_{23}	U_{23}
Ge(3)	0.0148(7)	0.0156(8)	0.0147(7)	0.000	0.000	0.0012(4)

respectively. More details of the data collection and the refinement parameters are given in the ESI.†

According to the results of the EDS measurements and the refinement results of SCXRD (atomic occupancies shown in Tables 4–6), the unit cell formulas of BCG's are derived to be: $Ba_8Cu_{5.1}Ge_{40.5}$ (BCG-Bi), $Ba_8Cu_{4.6}In_{1.4}Ge_{40.0}$ (BCG-In) and $Ba_8Cu_{5.1}Ge_{40.2}Sn_{0.7}$ (BCG-Sn) for the compounds grown by Bi-, In- and Sn-flux, respectively. Due to Zintl phase, the charge balance of a stoichiometric BCG can be expressed as,

$[Ba^{2+}]_8[(4b)Cu^{-3}]_{5.33}[(4b)Ge^0]_{40.67}$, where 4b means the sp^3-type 4 bonds. As a result of the charge balance, there are around 0.7, 0.8 and 0.7 additional electrons per unit cell as itinerant electrons for BCG-Bi, BCG-In and BCG-Sn, respectively. That is to say, the three compounds are expected to show similar carrier concentrations. Lattice constant is quite sensitive to the chemical composition as well. As In and Sn are included inside the crystal lattices, BCG-In and BCG-Sn show larger lattice constants than BCG-Bi and BCG-polycrystal, as can be seen in Table 2.

Disorder of the guest atom

The guest atom Ba(2) was found to be off-centered on the 24k site with a displacement of 0.173 Å and 0.155 Å from the center (the crystallographic 6d site) for BCG-Sn and BCG-In, respectively, as shown in Tables 4 and 5, while Ba2 is on-centered on the 6d site for BCG-Bi. Actually, a Ba(2) on-centered model can also be applied for the refinement of the X-ray diffraction data of BCG-Sn and BCG-In; but a slightly better result was obtained by using the off-centered model. The crystallographic information files (CIF) are provided in the Supporting Information for both cases. It should be noted that, different from BGSn,[4,30] the off-centered behavior can not be visualized by the electron density maps derived from the inverse Fourier transformation of the SCXRD data, because the off-centered displacements are too small. In the case of BCG-Bi, the off-centered model failed for refinement: even Ba(2) was intentionally moved to a 24k site or 24j cite at the beginning, it gradually recovered to the 6d site after several cycles of refinement. Interestingly, as the cage size increases from BCG-Bi to BCG-Sn and BCG-In, Ba2 becomes off-centered, this is consistent with our previous report that the potential inside the cage is very sensitive to the free space of the guest atom.[31] The guest atom vibrations are generally described by the Einstein model on solids, and the discussion will be given in the Heat capacity section.

Host site occupancy preference

As shown in Fig. 1, there are three crystallographic sites for host atoms: 6c, 16i and 24k. These atoms are arranged under the cubic space group, $Pm\bar{3}n$, to form both dodecahedral cages and tetrakaidecahedral cages. Generally, there are two ways to describe the framework structure. One was suggested by Demkov et al.[32] that the tetrakaidecahedral cages are joined together through their hexagonal faces to form pillars, which are arranged to construct the final structure (dodecahedral cages are the remained voids). The other description starts from the dodecahedral cages, which connect one another through the 16i site forming a scaffold structure with vacancies at the 6c site, and the tetrakaidecahedral cages would appear once these vacancies are filled with host atoms. The latter approach may help to explain the preference for vacancies and lower valence substitution elements (lower than the valence of the group 14 elements) on the 6c site.[21] It has been shown by early researches that direct bonds between lower valence elements are energetically unfavored, therefore the maximum occupancy factor (f) of the lower valence elements

on each site can be derived to be: $f(6c) < 100\%$, $f(16i) < 50\%$, $f(24k) < 50\%$, $f(6c + 24k) < 100\%$ and $f(16i + 24k) < 50\%$.[21] By applying the above principles under the Zintl Klemm concept, the number of substitution elements as well as their occupancy factors on each site can be roughly analysed. However, this is not enough for a clear understanding of the site occupancy character in the present study.

According to the structure parameters shown in Tables 4–6, the three framework sites are occupied differently for the compounds grown by different fluxes. In the case of BCG-In, the 6c site is fully occupied by Cu and In, while the other sites are uniformly occupied by Ge. During the structure refinement, any attempt of moving Cu/In to the 16i/24k site was failed. As for BCG-Sn, Cu substitutes Ge only on the 6c site, and Sn substitutes Ge only on the 24k site, Ge partially occupies the 6c and 24k sites and fully occupies the 16i site. The refinement with Sn on the 16i/6c site or Cu on the 16i/24k site was not successful. For BCG-Bi, the site occupancy factors are similar to that of BCG-Sn except that there is no Sn but a small mount of vacancies in the crystal lattice. It should be noted that, as the atomic form factors of Cu and Ge are similar, it is hard to distinguish them in the X-ray diffraction analyses, therefore the occupancy factor of Cu/Ge on the 6c site is set around 0.85/0.15, according to the EDS results.[23]

In order to interpret the site occupancy, we start from the crystal structure and especially focus on the tetrakaidecahedral cage. According to the distance from the cage center (the guest 6d site) to the cage atoms, there are four different atoms on the tetrakaidecahedral cage: 6c, 16i, 24k(1) and 24k(2) as shown in Fig. 1, in another word, there are four different cage radii. Fig. 3 shows the cage radii as well as their ratio to the lattice constant as a function of the lattice constant. 24k(1), which is on the six-member ring, is the nearest site from the center, while 24k(2) is the farthest. The cage radii $R_i(i = 1, 2, 3, 4)$ increase monotonically with the increase of their lattice constants. Distortions are observed for atoms on the 16i and 24k sites, especially the 24k site. There are two trends for the distortion. One is shown by the dashed lines in Fig. 3(b), along which the compounds are composed of different frameworks (Si-, Ge- or Sn-based framework), an enhancement of the lattice constant would lead to a faster increase of R_3 and R_4 while a slower increase of R_1. This indicates that large host atoms tend to make the framework an ellipsoid (anisotropic) while small host atoms tend to make it a ball (isotropic). We can test this idea by taking $Ba_8Ga_{16}Si_{30}$ (BGSi), BGG and BGSn as examples. The other trend is shown by the empty symbols with cross inside for NS, KS and BS with the same Si-based framework. As the lattice constant increases, R_1, R_3 and R_4 show an opposite trend of changes from the trend 1, which is shown by dashed lines. This reveals that large guest atoms tend to make the framework a ball, while small guests tend to make it an ellipsoid. In addition, previous report showed that the distortion of each site can also be examined by bond angle.[18] The bond angle around the 6c site is the closest to the angle of the regular tetrahedron, while the bond angle around the 24 site has the largest deviation. (One can refer to the CIF for details in the ESI†)
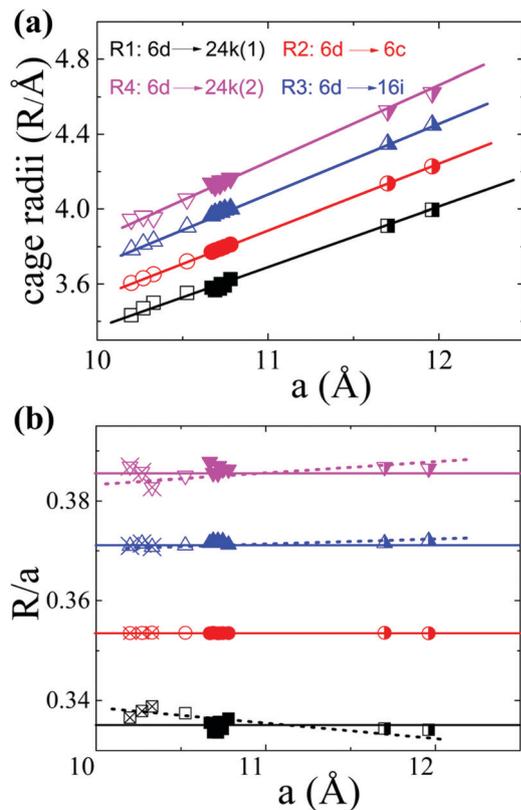
Fig. 3 The tetrakaidecahedral cage radii of different type-I clathrates. (a) The relationship between the cage radii and the lattice constant. (b) The ratio of the cage radii to their lattice constant as a function of the lattice constant. Empty symbols represent Si-based clathrate, filled symbols represent Ge-based clathrate and half-filled symbols represent Sn-based clathrate. The empty symbols with cross inside are those compounds with the same Si-framework but different guest atoms: Na_8Si_{46} (NS), K_8Si_{46} (KS) and Ba_8Si_{46} (BS). Lines are guides for the eyes. The lattice parameters and structure information are take from ref. 4, 33, 34, 35 and 36] except the data of BCG's.

Based on the above discussions, the preferential occupancy on each site for BCG's can be well analysed. For the substitution of Ge by a small amount of Sn, the mismatch of the covalent radii would create a local disorder, therefore the 24k site where distortions are frequently observed is most suitable for Sn. This is what we observed for BCG-Sn as shown in Table 4. For Cu substitution, it is energetically favored to occupy the 6c site as reported previously.[18,37] An alternative explanation is given here based on the R_i. According to the geometry of the tetrakaidecahedral cage, the 24k(1) and 6c sites are the closest to the guest atom at 6d site (electron donor), in principle lower-valence elements like Cu and vacancies, which behave like electron acceptors, should prefer to occupy the two sites for an easy charge transfer. However 24k(1) and 24k(2) are crystallographically the same site, and R_4 (the distance between the 6d site and 24k(2) site) is the longest cage radius, the averaged distance from 24k to 6d is farther than that from 6c to 6d. Therefore 6c site would be more favored for lower valence elements or vacancies. The situation for In substitution is slightly complicated: on one hand, the lower valence In should

occupy the 6c site; while on the other hand, due to the size mismatch of In and Ge, In should occupy the 24k site. It seems that In on the 6c site gives a more stable structure, because the refinement with In on the other two sites was failed.

Comparing to other type-I clathrates, the framework structure of BCG is relatively more ordered, because the substitution element (Cu) prefers to occupy 6c site and the number of Cu is close to 6 (a full occupation of the 6c site). In particular for BCG-In, where the 6c site is full occupied by Cu and In, leaving the other two sites fully and uniformly occupied by Ge. As to BCG-Bi, vacancies have been observed on the framework, and this is a common problem for Ge-based ternary clathrates, possibly inherited from the mother compound Ba_8Ge_{43}.[18,21,38] The slightly larger ADP values for BCG-Bi may indicate a structure disorder. For BCG-Sn, Sn on the 24k site may also create a small local disorder. It will be shown later that the framework structure is closely associated with the electrical transport properties in type-I clathrate, and it can be visualized by the single crystals work in the present study.

Electronic band structure

Band structure calculations were performed based on the experimental obtained crystal structure using the same method as we did in our previous report.[23] Fig. 4 shows the calculation results for different Cu containing clathrates, where Cu and In are on the 6c site and Sn is on the 24k site. The results are consistent with the Zintl concept that $Ba_8Cu_6Ge_{40}$ is a p-type compound, $Ba_8Cu_5Ge_{40}Sn_1$ is an n-type compound and $Ba_8Cu_5Ge_{40}In_1$ is an intrinsic semiconductor. The overall band features for the three cases are not quite different, especially that the lowest conduction bands are almost identical. Therefore, if the Fermi level are located at similar positions of the conduction band (n-type with similar carrier concentrations), the three compounds should show similar electrical properties.

Carrier concentration and electrical transport properties

Hall resistivity measurements show that all the BCG single crystals are n-type. The carrier concentration from 2 K to 300 K, derived from the Hall coefficient using a single band model, is shown in Fig. 5(a), and it is almost temperature independent. Interestingly, the three compounds have the same carrier type and a similar conduction band (Fig. 4) with a similar density of carriers, therefore, as we mentioned earlier, they shall behave similarly in electrical properties, unless some extrinsic factors such as grain boundary and structure disorder may exert a large influence. The electrical resistivity of BCG compounds is shown in Fig. 5(b), where all the compounds give a metallic conduction behavior. The electrical mobility was derived using $\mu = 1/ne\rho$ and the result is given in Fig. 5(c). It is shown that the mobility decreases as temperature increases, and the behavior demonstrates that the electron scattering process is dominated by electron–phonon scattering. A small influence from ionic impurity scattering was observed below 50 K for BCG-In compounds, possibly because the electron–phonon scattering weakens at that low temperatures. It should be noted that the electrical resistivity is mainly controlled by the electrical
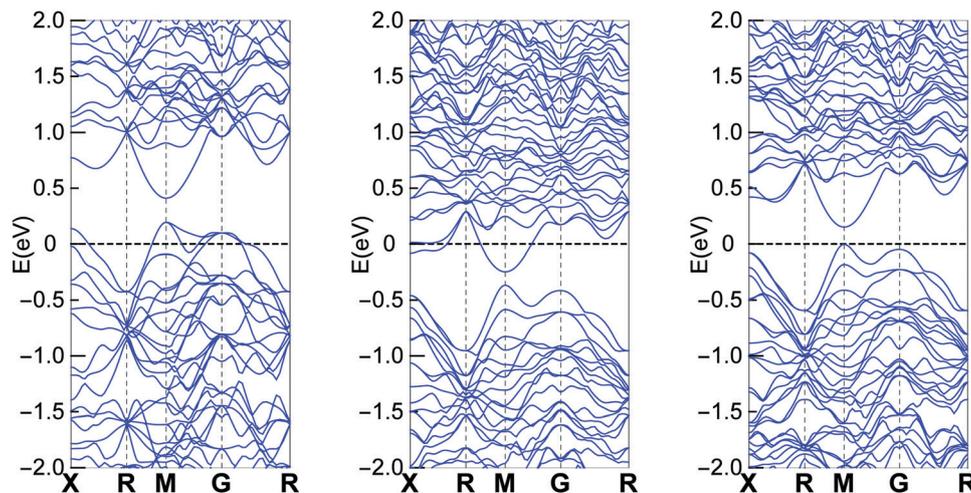
Materials Advances

Fig. 4 Band structure of $Ba_8Cu_6Ge_{40}$ (left), $Ba_8Cu_5Ge_{40}Sn_1$ (middle) and $Ba_8Cu_5Ge_{40}In_1$ (right). Part data of $Ba_8Cu_6Ge_{40}$ and $Ba_8Cu_5Ge_{40}Sn_1$ were published in our previous report.[23]

mobility *via* $\rho = 1/ne\mu$ for these compounds as shown in Fig. 5(d), because the values of n are quite close for these samples.

Fig. 6 shows the RT electrical mobility obtained in the present study as well as from literatures[17,39] for comparison. Our single crystals have much higher electrical mobility, especially for BCG-In compounds. A value of 44.8 cm^2 V^{-1} s^{-1}, which is almost the highest value at this carrier concentration

and 300 K, was obtained. According to effective mass approximation, electrical mobility can be written as $\mu = e\tau/m^*$, where τ is the electron scattering relaxation time and m^* is the electron effective mass. A large mobility can be obtained *via* a small m^* or a large τ. The band structure (Fig. 4) shows that the effective masses of BCG-In, BCG-Sn and BCG-Bi should be similar (it will be shown in the next section that the effective masses are indeed similar), so the difference of the mobility in
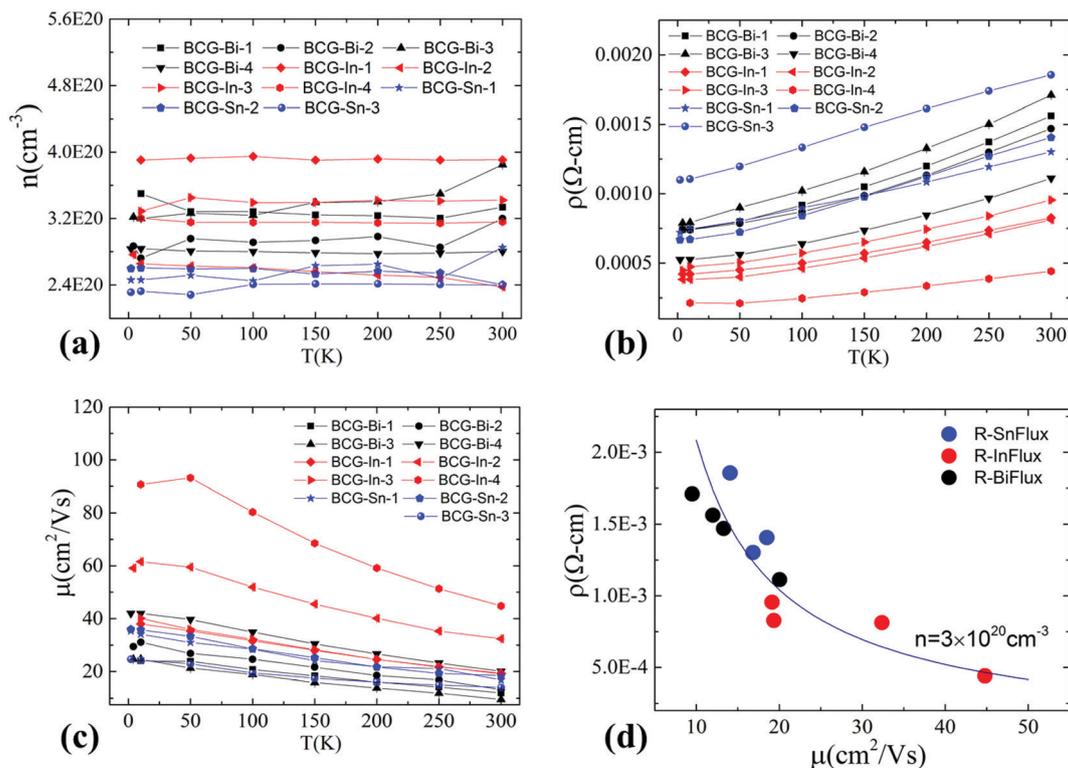

Fig. 5 Charge carrier concentration and electrical transport properties of BCG single crystals grown by In-, Sn- and Bi-flux. (a) Carrier concentration. (b) Electrical resistivity. (c) Electrical mobility. (d) Mobility dependent resistivity at 300 K. The curve in (d) is fitted using the free electron model with $n = 3 \times 10^{20}$ cm^{-3}.
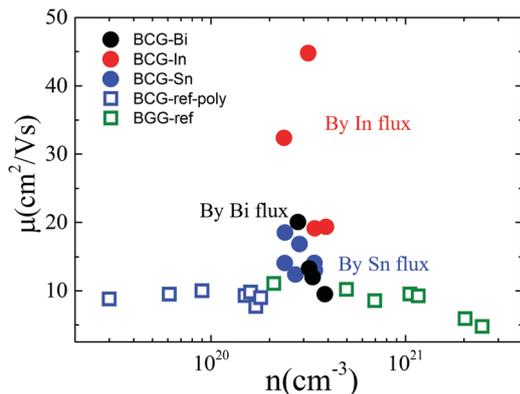
Fig. 6 The relationship of electrical mobility and carrier density at 300 K. The empty symbols are the data from ref. 17 and 39 for BCG and BGG compounds.

Fig. 6 is merely the result of the difference of τ for each sample. According to Matthiessen's rule, τ can be expanded as, $\tau_{tot}^{-1} = \tau_{ph}^{-1} + \tau_{defect}^{-1} + \tau_{impurity}^{-1} + \tau_{boundary}^{-1}$, where τ_{ph}, τ_{defect}, $\tau_{impurity}$ and $\tau_{boundary}$ are the relaxation times due to electron–phonon scattering, electron-defect scattering, electron-impurity scattering and electron-boundary scattering, respectively. For polycrystal compounds, conduction electrons suffer a lot of grain-boundary scattering, so they show much lower mobilities.[17,39] In type-I clathrate, electrons also suffer a lot of point-defect scattering due to the structure disorder, and the electrical mobility is largely restricted.[12,14,40] It was discussed earlier that structure disorder might be minimized in BCG, because the 6c site is almost fully occupied by Cu, leaving the 24k and 16i sites uniformly occupied by Ge. This could be the reason that we observed high mobilities for our BCG single crystals grown out of metal fluxes. In particular, BCG-In has the highest mobility and most ordered framework structure. It will be shown later that the high electrical mobility will be very significant for improving thermoelectric performance.

Heat capacity

The heat capacity data of BCG compounds are shown in Fig. 7, where low-energy excitation peaks arising from guest-atom

vibrations can be clearly seen. Generally, guest atoms are modeled as Einstein oscillators while the framework atoms are treated as the Debye oscillators. By applying the Einstein and Debye models on solids with two Einstein temperatures (θ_{E1} and θ_{E2}) and one Debye temperature (θ_D), the heat capacity data with low-energy excitation peaks (Fig. 7(a)) can be well fitted. The fitting method has been described in details in our previous report.[31] The fitting parameters are given in Table 7. The Einstein temperatures of BCG-In are a little bit smaller than those of other BCG compounds, this is most likely the result of the larger size of BCG-In (Table 2).

The above non-linear fitting based on the quasi-harmonic model indicates that BCG compounds do not show large anharmonicity of the guest-atom vibrations. Under the harmonic model, heat capacity (C_p) of solids can be expressed as, $C_p = \gamma T + DT^3$ below 3 K. Here γT is the temperature linear dependent heat capacity due to conduction carriers or tunneling states,[13] and DT^3 is the heat capacity described by the Debye T^3 law. According to Fig. 7(b), γ can be derived from the intercept in the linear fitting, and the values are listed in Table 7. The values of γ_{free-e}, calculated by using the free electron model: $\gamma_{free-e} = k_B^2 m_e (3\pi^2 n)^{1/3}/(3\hbar^2)$, are also given in the table for comparison. In the above equation, k_B is the Boltzmann constant, $\hbar$ is the reduced Planck constant, m_e is the free electron mass, and n is the carrier concentration. Effective mass of conduction carriers (m^*) was calculated by γ/γ_{free-e}. As mentioned earlier, the m^*'s of BCG-In and BCG-Sn are indeed similar, and the values are also very close to the values of reported BCG and BGG compounds.[13,17]

Thermoelectric properties

Thermoelectric parameters (ρ, S, κ and ZT) as a function of temperature are shown in Fig. 8. The error bars, from several measurements, are also shown in Fig. 8. The negative Seebeck coefficients indicate that the compounds are of n-type conduction, which is in agreement with the Hall measurements described earlier. The Seebeck coefficients of the compounds in the present work are very close, because the samples have a similar n as well as a similar m^*. Under the effective mass approximation, it is possible
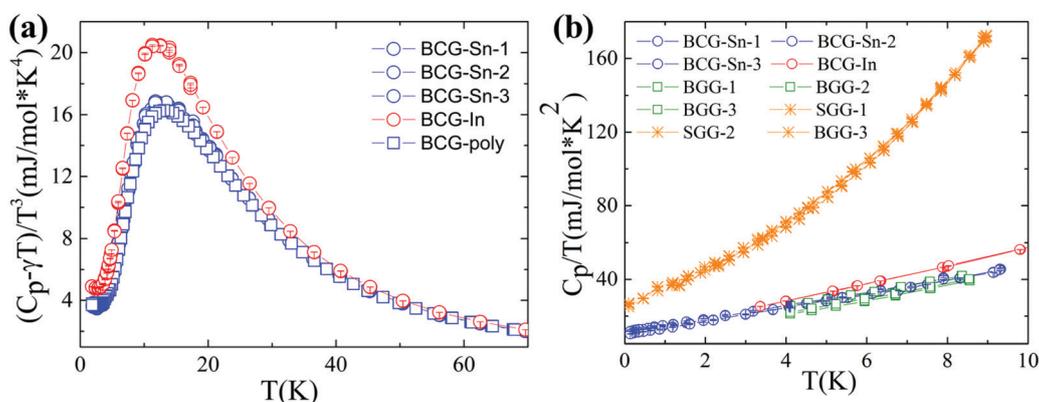

Fig. 7 Heat capacity data of BCG-In and BCG-Sn single crystals as well as BCG polycrystals. (a) $(C_p - \gamma T)/T^3$ vs. T plot, where γT is the temperature linear dependent heat capacity contributed from conduction carriers. (b) C_p/T vs. T^2 plot below 3 K, for comparison, the data of BGG and SGG are also included.[13]

Table 7 The fitting parameters of heat capacity: Debye (θ_D) and Einstein temperatures (θ_{E1} and θ_{E2}) and γ. $\gamma_{\text{free-e}}$ is calculated based on the free electron model as described in the text

Sample	θ_{E1}/K	θ_D/K	θ_{E2}/K	γ/mJ mol^{-1} K^{-2}	$\gamma_{\text{free-e}}$/mJ mol^{-1} K^{-2}	m^*/m_e
BCG-Sn1	58	284	95	10.14	7.74	1.31
BCG-Sn2	58	284	95	11.27	7.90	1.43
BCG-Sn3	58	284	95	9.81	7.29	1.34
BCG-In	54	264	90	8.78	7.31	1.20
BCG-poly	58	284	95	—	—	1.0–1.2[17]

to write S as,

$$S = \frac{2\pi^2}{3\hbar^2}\frac{k_B}{e}k_B T m^* \left(\frac{1}{3\pi^2 n}\right)^{2/3} \tag{1}$$

From the linear fitting of the temperature dependent S, m^* was derived to be $1.43m_e$, $1.39m_e$, $1.31m_e$, and $1.41m_e$ for BCG-Sn1, BCG-Sn2, BCG-Sn3, and BCG-In, respectively. These values are very close to the values calculated from heat capacity, as shown in Table 7. All BCG compounds show very low κ as a result of the rattling phonon modes of the guest atoms. Radiation losses were observed at around RT and they were empirically corrected by referring to the data in our previous report.[23] The figure of merit ZT was calculated using $ZT = (S^2\sigma/\kappa)T$, and the result is shown in Fig. 8(d). The highest ZT value, which achieves 0.1 at 300 K, is much higher than the values of reported polycrystals.[17] It will be shown in the following part that the high ZT values are achieved mainly due to the high electrical mobility of the BCG single crystals.

We start from the n dependent thermoelectric parameters at 300 K as shown in Fig. 9. The Seebeck coefficient decreases monotonically as n increases in accordance with $S \propto T m^* n^{-2/3}$. The monotonic behavior of $S(n)$ indicated by the fitting curves in Fig. 9(a) demonstrates that the m^* of BCG and BGG are very close to each other. It is obvious that S is not sensitive to μ for the compounds in the present study. However, PF, which can be expressed by PF $= S^2\sigma = S^2 n e \mu$, should be strongly dependent on μ. As shown in Fig. 9(b), the PF's of our single crystals is much higher than the previous reported data.[14,17,39] In the marked region, where the variation of n is very small, the influence of other factors except n is obvious, and the influence is mainly due to μ.

In order to derive the relationship between PF and μ, the samples were cut into small pieces after thermal transport measurements, and μ for each piece was deduced by electrical transport measurements. For one sample, each piece shows different μ, therefore the averaged μ with error bars was applied for the following analyses. As shown in Fig. 10, PF increases almost linearly as μ increases, which is consistent with the
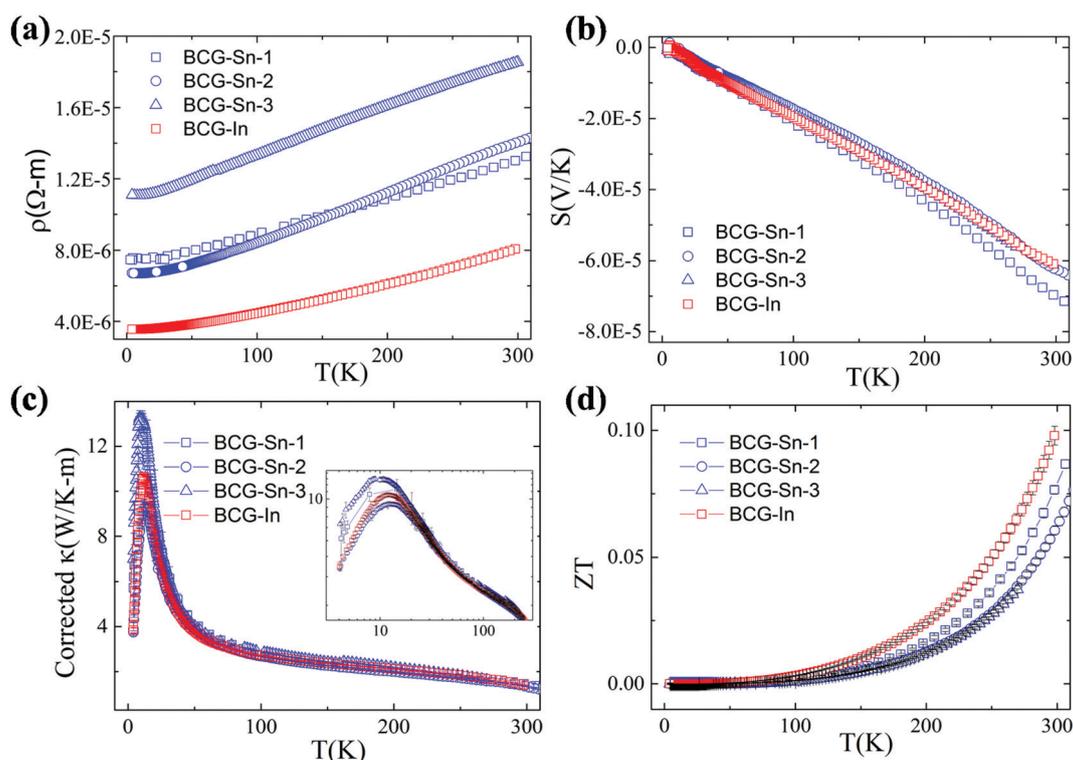

Fig. 8 Thermoelectric properties of BCG-Sn and BCG-In single crystals from 2 K to 300 K. (a) Electrical resistivity. (b) Seebeck coefficient. (c) Thermal conductivity after the correction of radiation losses. The inset shows the original thermal conductivity data. (d) The figure of merit ZT.
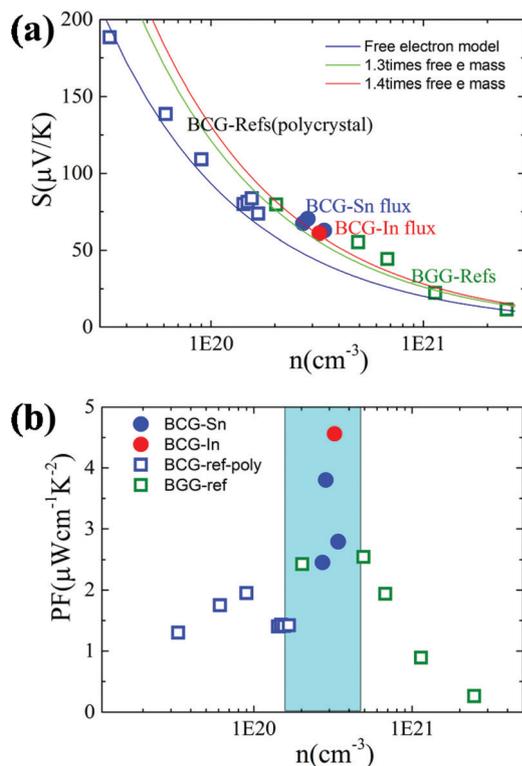
Fig. 9 (a) The relationship between S and n at 300 K. The fitting curves were made under the effective mass approximation with different effective masses. (b) The relationship between PF and n at 300 K. The data of BGG and BCG polycrystals are taken from ref. 14, 17 and 39.
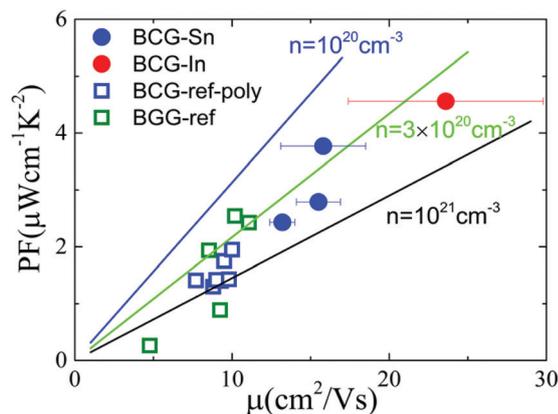

Fig. 10 The influence of μ on thermoelectric parameters. (a) The relationship between PF and μ at 300 K. The linear lines were plotted under the effective mass approximation with $m^* = 1.3$. (b) The relationship between nS^2 and μ at 300 K. The thick arrows are the guides for the eyes. The error bar of μ arises from the inhomogeneity of the sample in the thermal transport measurement. The data of BGG and BCG polycrystals are taken from ref. 14, 17 and 39.

simple model in the metallic limit under the effective mass approximation,

$$PF = \frac{4\pi^4}{9\hbar^4}\frac{k_B^4}{e}\frac{1}{(3\pi^2)^{4/3}}T^2 m^{*2} n^{-1/3}\mu \qquad (2)$$

where T is 300 K, m^* and n are almost constants. Now it is clear that an enhancement of μ will give rise to an enhancement of PF as well as ZT for clathrate compounds.

As shown in eqn 2, PF can be enhanced through m^*, n, and μ, which correlates with each other. Normally, m^* is decided by the band structure. n is widely used to tune thermoelectric properties through doping. And μ is affected by different scattering. For n-type clathrate single crystal, the disorder in the cage framework might be most important for μ. As can be seen in Tables 4 and 5, BCG-In is less disorder in 24k sites, which gives a high μ. Accordingly, if less disorder is found in 6c sites, a higher μ might be obtained, leading to better thermoelectric performance.

Conclusion

Single crystals of Cu containing clathrates (BCG-In, BCG-Sn, and BCG-Bi) were successfully synthesized by using different metal fluxes. The selected compounds were characterized by powder and single crystal X-ray diffraction measurements, SEM-EDS measurements, and physical properties measurements. A small amount of Sn was observed on the 24k site for BCG-Sn, and a small amount of In was observed on the 6c site for BCG-In, while no Bi was observed for BCG-Bi. The origin of host site preference was discussed. As a result of the high crystal quality and the ordered cage framework, the compounds in the present study showed very high electrical mobility: 44.8 cm^2 V^{-1} s^{-1} at 300 K for BCG-In, almost five times higher than the reported values of BCG polycrystals at the same carrier concentration. High electrical mobility was shown to enhanced the thermoelectric power factor, PF, as well as the figure of merit, ZT, which was derived to be 4.6 μW cm^{-1} K^{-2} and 0.1, respectively, for the BCG-In compound at 300 K. Our results did not only provide a guideline for optimizing ZT via μ in type-I clathrates, but also showed that Sn-, In-, and Bi-flux could be widely applied to grow single crystals of other transition elements containing clathrates.

Conflicts of interest

There are no conflicts to declare.

Acknowledgements

References

1 *Thermoelectrics Handbook*, ed. D. M. Rowe, CRC Press, Taylor & Francis Group, 2006.

2 A. Saramat, G. Svensson, A. E. C. Palmqvist, C. Stiewe, E. Mueller, D. Platzek, S. G. K. Williams, D. M. Rowe, J. D. Bryan and G. D. Stucky, *J. Appl. Phys.*, 2006, **99**, 023708.

3 T. Takabatake, K. Suekuni, T. Nakayama and E. Kaneshita, *Rev. Mod. Phys.*, 2014, **86**, 669–716.

4 J. Wu, J. Xu, D. Prananto, H. Shimotani, Y. Tanabe, S. Heguri and K. Tanigaki, *Phys. Rev. B: Condens. Matter Mater. Phys.*, 2014, **89**, 214301.

5 *The Physics and Chemistry of Inorganic Clathrates*, ed. G. S. Nolas, Springer, Netherlands, 2014.

6 J. L. Cohn, G. S. Nolas, V. Fessatidis, T. H. Metcalf and G. A. Slack, *Phys. Rev. Lett.*, 1999, **82**, 779–782.

7 M. Christensen, A. B. Abrahamsen, N. B. Christensen, F. Juranyi, N. H. Andersen, K. Lefmann, J. Andreasson, C. R. H. Bahl and B. B. Iversen, *Nat. Mater.*, 2008, **7**, 811–815.

8 S. Pailhès, H. Euchner, V. M. Giordano, R. Debord, A. Assy, S. Gomès, A. Bosak, D. Machon, S. Paschen and M. de Boissieu, *Phys. Rev. Lett.*, 2014, **113**, 025506.

9 T. Tadano, Y. Gohda and S. Tsuneyuki, *Phys. Rev. Lett.*, 2015, **114**, 095501.

10 S. M. Dresselhaus, G. Chen, M. Y. Tang, R. Yang, H. Lee, D. Wang, Z. Ren, J.-P. Fleurial and P. Gogna, *Adv. Mater.*, 2007, **19**, 1043–1053.

11 M. G. Kanatzidis, *Chem. Mater.*, 2010, **22**, 648–659.

12 H. Zhang, H. Borrmann, N. Oeschler, C. Candolfi, W. Schnelle, M. Schmidt, U. Burkhardt, M. Baitinger, J.-T. Zhao and Y. Grin, *Inorg. Chem.*, 2011, **50**, 1250–1257.

13 J. Xu, J. Tang, K. Sato, Y. Tanabe, H. Miyasaka, M. Yamashita, S. Heguri and K. Tanigaki, *Phys. Rev. B: Condens. Matter Mater. Phys.*, 2010, **82**, 085206.

14 S. Johnsen, A. Bentien, G. K. H. Madsen, M. Nygren and B. B. Iversen, *Phys. Rev. B: Condens. Matter Mater. Phys.*, 2007, **76**, 245126.

15 X. Shi, J. Yang, S. Bai, J. Yang, H. Wang, M. Chi, J. R. Salvador, W. Zhang, L. Chen and W. Wong-Ng, *Adv. Funct. Mater.*, 2010, **20**, 755–763.

16 M. Hokazono, H. Anno and K. Matsubara, *Mater. Trans.*, 2005, **46**, 1485–1489.

17 S. Johnsen, A. Bentien, G. K. H. Madsen, B. B. Iversen and M. Nygren, *Chem. Mater.*, 2006, **18**, 4633–4642.

18 E. Alleno, G. Maillet, O. Rouleau, E. Leroy, C. Godart, W. Carrillo-Cabrera, P. Simon and Y. Grin, *Chem. Mater.*, 2009, **21**, 1485–1493.

19 X. Yan, M. Ikeda, L. Zhang, E. Bauer, P. Rogl, G. Giester, A. Prokofiev and S. Paschen, *J. Mater. Chem. A*, 2018, **6**, 1727–1735.

20 X. Yan, E. Bauer, P. Rogl, J. Bernardi, A. Prokofiev and S. Paschen, *Z. Anorg. Allg. Chem.*, 2020, **646**, 1055–1061.

21 M. Christensen, S. Johnsen and B. B. Iversen, *Dalton Trans.*, 2010, **39**, 978–992.

22 M. Ikeda, X. Yan, L. Prochaska, G. Lientschnig, R. Svagera, M. Waas, P. Tomes, A. Prokofiev, E. Bauer and S. Paschen Thermal conductivity of transition metal containing type-I clathrates. Symposium S/W/CC - Advanced Materials for Photovoltaic, Fuel Cell and Electrolyzer, and Thermoelectric Energy Conversion. 2015.

23 J. Xu, J. Wu, H. Shao, S. Heguri, Y. Tanabe, Y. Liu, G. Liu, J. Jiang, H. Jiang and K. Tanigaki, *J. Mater. Chem. A*, 2015, **3**, 19100.

24 A. C. Larson and R. B. Von Dreele, *Los Alamos Natl. Lab.*, 1994, **86**, 748.

25 B. H. Toby, *J. Appl. Crystallogr.*, 2001, **34**, 210–213.

26 L. J. Farrugia, *J. Appl. Crystallogr.*, 2012, **45**, 849–854.

27 G. Kresse and J. Furthmüller, *Phys. Rev. B: Condens. Matter Mater. Phys.*, 1996, **54**, 11169–11186.

28 G. Kresse and D. Joubert, *Phys. Rev. B: Condens. Matter Mater. Phys.*, 1999, **59**, 1758–1775.

29 J. P. Perdew, K. Burke and M. Ernzerhof, *Phys. Rev. Lett.*, 1996, **77**, 3865–3868.

30 K. Suekuni, M. A. Avila, K. Umeo, H. Fukuoka, S. Yamanaka, T. Nakagawa and T. Takabatake, *Phys. Rev. B: Condens. Matter Mater. Phys.*, 2008, **77**, 235119.

31 J. Wu, K. Akagi, J. Xu, H. Shimotani, K. K. Huynh and K. Tanigaki, *Phys. Rev. B*, 2016, **93**, 094303.

32 A. A. Demkov, O. F. Sankey, K. E. Schmidt, G. B. Adams and M. O'Keeffe, *Phys. Rev. B: Condens. Matter Mater. Phys.*, 1994, **50**, 17001–17008.

33 O. O. Kurakevych, T. A. Strobel, D. Y. Kim, T. Muramatsu and V. V. Struzhkin, *Cryst. Growth Des.*, 2013, **13**, 303–307.

34 S. Stefanoski and G. S. Nolas, *Cryst. Growth Des.*, 2011, **11**, 4533–4537.

35 S. Yamanaka, E. Enishi, H. Fukuoka and M. Yasukawa, *Inorg. Chem.*, 2000, **39**, 56–58.

36 A. Bentien, E. Nishibori, S. Paschen and B. B. Iversen, *Phys. Rev. B: Condens. Matter Mater. Phys.*, 2005, **71**, 144107.

37 K. Moriguchi, S. Munetoh, A. Shintani and T. Motooka, *Phys. Rev. B: Condens. Matter Mater. Phys.*, 2001, **64**, 195409.

38 U. Aydemir, C. Candolfi, H. Borrmann, M. Baitinger, A. Ormeci, W. Carrillo-Cabrera, C. Chubilleau, B. Lenoir, A. Dauscher, N. Oeschler, F. Steglich and Y. Grin, *Dalton Trans.*, 2010, **39**, 1078–1088.

39 H. Anno; M. Hokazono; M. Kawamura and K. Matsubara, Effect of transition element substitution on thermoelectric properties of semiconductor clathrate compounds. Thermoelectrics, 2003 Twenty-Second International Conference on – ICT, 2003, pp. 121–126.

40 B. Du, Y. Saiga, K. Kajisa and T. Takabatake, *Chem. Mater.*, 2015, **27**, 1830–1836.